

Tunneling through nanographene stacks

F. Jäckel,¹ M. D. Watson,^{2,3} K. Müllen,² and J. P. Rabe^{1,*}

¹*Department of Physics, Humboldt University Berlin, Newtonstraße 15, 12489 Berlin, Germany*

²*Max Planck Institute for Polymer Research, Ackermannweg 10, 55128 Mainz, Germany*

³*Department of Chemistry, University of Kentucky, Lexington, Kentucky 40506-0055, USA*

(Received 2 September 2005; published 19 January 2006)

We present a scanning tunneling microscopy (STM) and spectroscopy (STS) study of a nanographene, hexa-*peri*-hexabenzocoronene (HBC), in different stacked geometries, covalently bound in cyclophanes or physisorbed in double layers consisting either of HBCs only or of a mixture of HBC and an alkylated disk-type electron acceptor, coronenediimide. Tunneling bias-dependent STM and STS at the solid-liquid interface reveal that the lateral offset between the stacked molecules strongly influences the electron transport through the stacks, which is attributed to different highest occupied and lowest unoccupied molecular orbital splittings in the stacks. The results imply that the control over the stacking in nanographene multilayers or columns can be used to control their electron transport properties.

DOI: [10.1103/PhysRevB.73.045423](https://doi.org/10.1103/PhysRevB.73.045423)

PACS number(s): 73.40.Gk, 73.20.Hb, 81.07.Nb, 85.65.+h

I. INTRODUCTION

The paper of Aviram and Ratner¹ on a rectifier, based on a single molecule, to the best of our knowledge, gave birth to the field of molecular electronics and stimulated remarkable theoretical and experimental progress towards this potential alternative to inorganic semiconductor-based nanoelectronics.²⁻⁴ A number of techniques has been applied to the study of the electron transport properties of single molecules or small ensembles, thereof, including scanning tunneling microscopy and spectroscopy (STM/STS),⁵⁻⁹ conductive probe scanning force microscopy,¹⁰ mechanically controlled break-junctions,^{11,12} and nanofabricated pores.¹³ Also three-terminal devices, i.e., transistors, have been made from carbon nanotubes^{14,15} or single molecules.^{16,17} Even though the gap between the electrodes can be controlled in all these approaches on the nanometer scale, the electrodes themselves are meso- or macroscopic. However, one can only profit from the molecular scale of the active components in molecular electronic devices if the control of the electronic properties of single molecules is exercised by the immediate environment of the molecule, thus leading to true monomolecular electronics.^{2,18} To correlate the electronic properties of a single molecule with its immediate environment, i.e., neighbors, adsorption site, conformation, etc., electron transport measurements need to be combined with high-resolution spatial imaging which makes combined (STM/STS) studies the method of choice. Recent reports on the impact of π - π -interactions on molecular electronic properties include photoelectron emission studies on thin films of large planar polycyclic aromatic hydrocarbons,¹⁹ electron transport studies through monolayers of phenylene vinylene derivatives,²⁰ and scanning tunneling spectroscopy investigations of single pyrene and oligothiophene stacks *perpendicular* to the stacking direction assuming a single specific stacking geometry.^{21,22}

Here we present an STM and STS study of hexa-*peri*-hexabenzocoronenes (HBCs) in a number of different stacking geometries at the solid-liquid interface. The electron transport properties of single stacks is measured *parallel* to

the stacking direction, i.e., along the stacks. HBC constitutes an extended polycyclic aromatic hydrocarbon and thus can be regarded as a molecularly defined graphene subunit, i.e., a nanographene. HBCs form columnar mesophases exhibiting high charge carrier mobilities along the columns²³ which can therefore be considered as self-assembling nanowires with pronounced π - π -interactions of valence electrons. In the present case HBCs are studied in various bilayer architectures, namely in covalently bound pairs (cyclophanes) and in physisorbed epitaxial double layers of both pure HBC or in mixtures with an electron acceptor (see Fig. 1 for chemical formulae). The HBC molecules in the top layers of the stacks exhibit markedly different electron transport properties in the junction of the STM depending on the architecture in which they are embedded. The data suggest that these differences originate from a difference in the lateral offset between the stacked molecules in the various architectures. The lateral offset determines the highest occupied and lowest unoccupied molecular orbital (HOMO and LUMO) splitting of the stacked molecules and thereby the electronic properties of the stacks in the gap. Thus the electron transport through stacked molecules can be controlled via different architectures which determine the electronic coupling between them.

II. EXPERIMENTAL

The syntheses of the HBC-cyclophane **1**, parent HBC **2**, and the electron acceptor coronenediimide **3** have been described elsewhere.²⁴⁻²⁶ The self-assembly properties of **1**, **2**, and equimolar mixtures of **2** and **3** as well as the electron transport properties of **1** have also been reported.^{24,27} However, as will be shown below, the previously suggested packing models cannot explain the electronic properties reported here and will, therefore, be modified. STM and STS measurements at solid-liquid interfaces²⁸ were performed using a home-built beetle-type STM interfaced with a commercial controller (Omicron). STM tips have been prepared by mechanically cutting a 0.25 mm diameter Pt/Ir (80%/20%) wire. Near-saturated solutions of the compounds under study

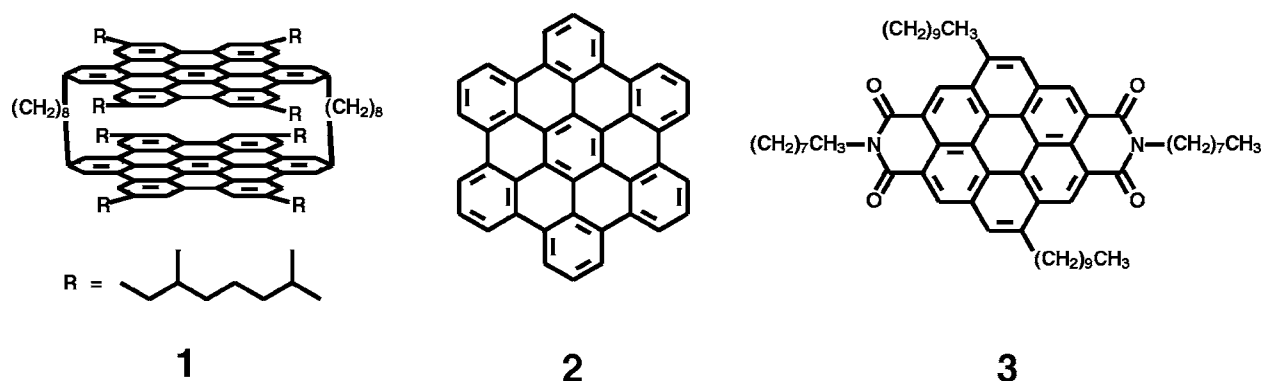


FIG. 1. Chemical formulae of the investigated molecules: an HBC-cyclophane **1**, unsubstituted HBC **2**, and a coronenediimide-derivative **3**.

in 1,2,4-trichlorobenzene were applied to the basal plane of freshly cleaved highly oriented pyrolytic graphite (HOPG). The neat HBC **2** could be sufficiently solubilized in hot (100 °C) trichlorobenzene or in equimolar mixtures with **3**.²⁷ STS measurements were performed by positioning the tip above the region of interest and running a voltage ramp with 100 equidistant values between -1.5 and 1.5 V with the feedback loop switched off. The tip-sample separation was determined by the parameters of the feedback-loop upon switching it off. Spectroscopic data were accepted only if imaging was stable with a typical contrast before and after STS measurements, and if there was no lateral shift between the images recorded with different scan directions. Finally, tunneling spectra of a number of molecules were averaged provided that they met the settings of the feedback loop with acceptable accuracy ($\pm 10\%$).

III. RESULTS AND DISCUSSION

A. HBC cyclophane

Figure 2(a) displays an STM current image of the HBC-cyclophane **1**. The bright circular spots corresponding to high tunneling probability are attributed to the conjugated cores of the HBC disks since the energetic difference between their frontier orbitals and the Fermi level of the sub-

strate are comparably small.²⁹ The dark areas corresponding to low tunneling probability are believed to be dynamically occupied by the alkyl substituents of **1** or solvent molecules which, due to their large HOMO-LUMO gap, do not give rise to detectable contributions to the tunneling current in this bias range. The two-dimensional lattice of **1** is a dimer structure described by a unit cell with parameters $a=(1.8\pm 0.1)$ nm, $b=(4.1\pm 0.15)$ nm, and $\alpha=(73\pm 2)^\circ$.²⁷ Figure 2(b) displays current-voltage characteristics measured through the conjugated HBC cores of **1**. The curve has marked asymmetry originating from the HOMO of the stack,^{5,30} with larger tunneling probability at negative sample bias. The I-Vs from areas attributed to alkyl chains from an alkylated HBC appear rather symmetrical and only reflect the remaining asymmetry of the tunneling junction, i.e., different electrode materials and shapes.^{5,30} In the following the cyclophane **1** will serve as a model. It has been concluded from a comparison of NMR studies of **1** in solution, with solid state NMR studies of **2**, that the intramolecular disk-disk offset of the former is not larger than for **2** in the bulk.²⁴ For single crystals of **2** this center-to-center lateral offset has been reported to be 0.38 nm from x-ray diffraction measurements³¹ which is about one-third of the disk's diameter. In the following we assume that this small lateral offset in the cyclophanes does not change upon adsorption due to the covalent connection of the disks.

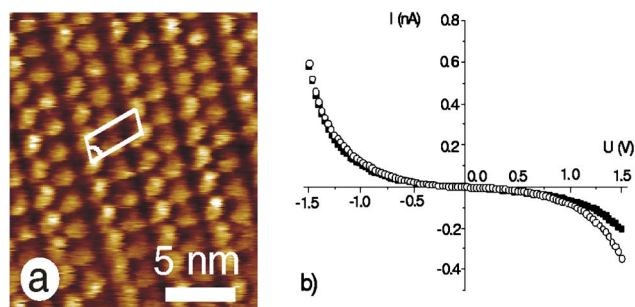


FIG. 2. (Color online) (a) An STM current image of a highly ordered monolayer of **1** exhibiting a dimer arrangement (sample bias $U_s=-1.4$ V and average tunneling current $I_t=50$ pA). (b) Current-voltage characteristics through aromatic cores of **1** (solid symbols, average over 39 single curves) and through alkyl chain regions of an alkylated HBC (open symbols, 88 single curves).

B. Neat HBC

The unsubstituted HBC **2** is vanishingly soluble in hot trichlorobenzene (100 °C), but sufficiently so to allow visualization at the solid-liquid interface. Figure 3 displays STM current images obtained from such a solution. At small tunneling junction impedances (below $10^9 \Omega$) a periodic hexagonal pattern can be visualized with a lattice constant of 1.4 ± 0.1 nm [Fig. 3(a)].²⁷ The unit cell vectors of this lattice are rotated by 9° with respect to the zig-zag-direction of the underlying HOPG. Due to a strong adsorbate-substrate interaction it is difficult to recognize single HBC molecules in this pattern. However, the periodic pattern is indistinguishable from the one found for the same molecule on HOPG under ultra-high vacuum (UHV) conditions³² and is therefore attributed to a hexagonally close-packed layer of HBC. At

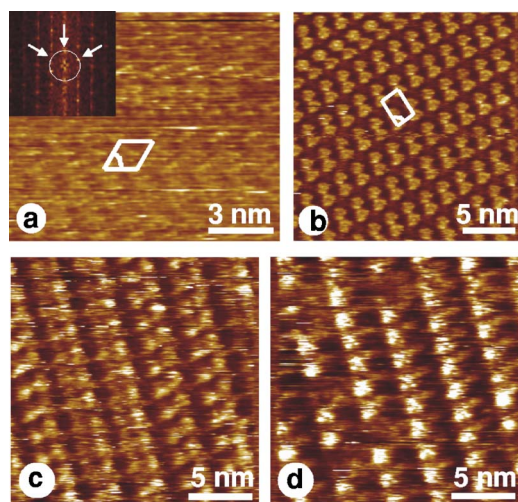


FIG. 3. (Color online) STM current images of the highly ordered double layer architecture obtained from **2**; (a) the first layer exhibiting a hexagonal arrangement as evidenced by the two-dimensional Fourier transformation in the inset ($U_s = -0.25$ V and $I_t = 600$ pA). (b) The second layer exhibiting a dimer arrangement ($U_s = -1.2$ V and $I_t = 100$ pA). (c) and (d) The dimer arrangement simultaneously imaged at opposite sample bias -1.4 V and $+1.4$ V, demonstrating a strong bias dependency of the relative contrast between the two HBC forming a dimer.

larger tunneling junction impedances (above $10^9 \Omega$), i.e., at larger tip-sample-separations, a different packing is observed [Fig. 3(b)]. This arrangement can be described by a unit cell containing two molecules and exhibiting parameters of $a = (3.3 \pm 0.2)$ nm, $b = (1.8 \pm 0.2)$ nm, and $\alpha = (86 \pm 5)^\circ$. Noteworthy, the electronic structure of the molecules in this arrangement appears much less disturbed than that observed at low tunneling impedances which indicates a weaker electronic coupling to the substrate. Since changing the tunneling parameters and thereby adapting the tip-sample separation allows switching between the two arrangements, the dimer arrangement is attributed to a second layer on top of the hexagonally close-packed layer.²⁷ The lower symmetry of the upper layer demands that not all molecules occupy the same crystallographic positions relative to the ground layer.

Figures 3(c) and 3(d) display simultaneously recorded STM current images of the double layers from **2** with different parameters for forward and backward scan directions. Simultaneous recording with different parameters assures one that differences in relative contrast between the images are not related to changes in tip quality. At negative sample bias [Fig. 3(c)] all HBC molecules appear approximately equally bright, while at the opposite bias [Fig. 3(d)] the brightness strictly alternates with one row from each dimer row appearing very bright while the other one is almost invisible. The differences in the electronic properties of the HBCs forming each row within dimer rows is more objectively demonstrated by STS (Fig. 4). While the I-Vs through the HBCs, which are dim at positive sample bias are indistinguishable from the model cyclophane **1**, an opposite asymmetry is observed in the I-Vs through the HBCs which appear bright at positive sample bias.

I-Vs through the HBCs in the first layer could not be measured with our present setup since, due to a limited dy-

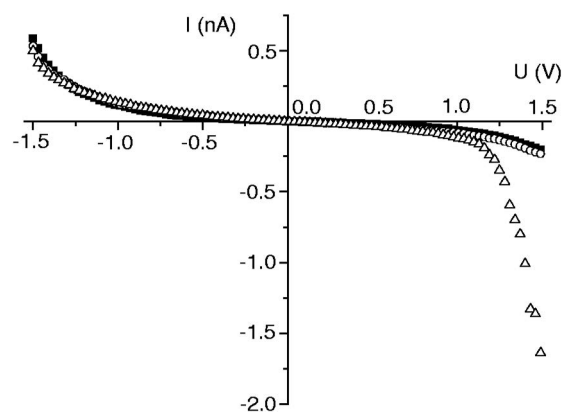


FIG. 4. I-Vs recorded at aromatic cores of **2** (open symbols, average over 20 and 12 single curves, respectively) in the dimer arrangement of the second layer grouped according to the position in the dimer compared to the I-Vs obtained from **1** (solid symbols) in the respective monolayers.

namic range of current detection STS measurements of the first layer can be carried out only for a limited bias range (± 0.3 V) which prohibits meaningful comparison with the double-layer data. Retracting the tip before measuring I-Vs seems to allow reformation of the double layer before the I-Vs are recorded. Such experiments, however, may be performed under UHV-conditions.

As stated above, and in previously suggested packing models,²⁷ not all of the molecules in the second layer can occupy crystallographically identical positions relative to the ground layer lattice due to a symmetry mismatch.

Interaction between identical conjugated molecules leads to shifts of the energy of molecular orbitals. Calculations³³ predict that the corresponding HOMO and LUMO splittings of conjugated molecules strongly depend on the intermolecular distance and the lateral displacement. The calculated HOMO and LUMO splitting for perfectly eclipsed, cofacial HBC dimers (interdisk distance of 0.35 nm) amounts to about 1.0 and 0.6 eV, respectively. These values are reduced to 0.5 and 0.3 eV when allowing for a lateral displacement between the disks as found in single crystals.³¹ We attribute the regularly variable electronic properties of the HBCs in the second layer to differing lateral offsets relative to the underlying HBCs which should correspond to different electronic coupling. This ultimately results in distinct differences in the HOMO- and LUMO-splittings which then give rise to the observed current-voltage characteristics. The fact that the I-Vs through HBCs, which appear dim at positive sample bias are indistinguishable from those of model **1** suggests similar electronic coupling and therefore similar lateral offsets. However, that does not mean necessarily that these “dim” HBCs occupy equivalent positions with respect to the first layer in a crystallographic sense. Only the overlap with the underlying disk is expected to be similar to **1**. For the cyclophane **1** it was stated previously that the lateral offset in the stack is not larger than in single crystals, i.e., not larger than a third of the disk’s diameter.²⁴ Since the π - π -interactions become more repulsive with greater overlap³⁴ it is suggested that these HBCs occupy positions with lateral displacements of 0.38 nm as reported for single

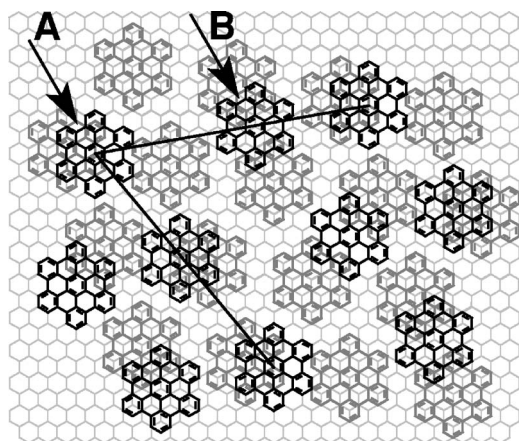


FIG. 5. Packing model for a double layer of **2**. The first and second layers are depicted in gray and black, respectively. The unit cell, taking into account inequivalent positions with respect to the first layer, is indicated as well as the rows which appear dim (*A*) and bright (*B*) at positive sample bias.

crystals. The unit cell of the second layer demands that the remaining HBCs (the “bright” rows) occupy positions with a larger lateral displacement with respect to their underlying disks.

A packing model reflecting the structure of the two layers which accommodates the variable interlayer electronic coupling is depicted in Fig. 5. In the ground layer, the HBC benzenoid rings are positioned relative to those of the HOPG in the same fashion as *A-B* stacked graphite. The unit cell and its relative orientation to HOPG are reproduced and scaled within the experimental accuracy (unit cell vector $a=1.4$ nm and is rotated 9° with respect to the HOPG lattice).

The second layer was constructed such that the lateral spacing of the molecules within each layer were reproduced within the experimental accuracy ($a=1.9$ nm, $b=3.2$ nm, and 82°). The exact positions of the molecules are fixed such that one row (indicated with *A*) from each dimer row contains

molecules that are laterally offset from the underlying molecules by 0.38 nm, the value reported for HBC single crystals.³¹ It is worth noting that this could only be achieved by applying different stacking patterns of the HBCs on the HOPG, namely alternating *A-B-A* and *A-B-C* stacks along this row. Taking this into account, a larger unit cell has to be used to describe the packing appropriately. The resulting lateral offset for the HBCs in the other row (indicated with *B*), relative to the underlying HBCs, is 0.62 nm and thus substantially larger than the bulk value. Interestingly, these HBCs must couple with two, rather than one, disks in the first layer. The larger tunneling probability at positive sample bias observed for molecules in rows *B* suggests larger HOMO- and LUMO-splittings than observed for rows *A*. The increase of tunneling probability at positive sample bias can then be explained by resonant contributions of the new LUMO if the HOMO-LUMO gap is narrowed by the larger splittings.

C. Mixtures of HBC **2** and coronenediimide **3**

Donor-acceptor interactions between the HBC **2** and the electron acceptor **3** allow codeposition without heating.²⁷ Deposition from an equimolar solution yields a double layer architecture at the solid-liquid interface. The ground layer is again the hexagonally close-packed layer of **2**. The second layer [Fig. 6(a)] can be described by an oblique unit cell containing four HBC molecules with parameters $a=(3.7\pm 0.3)$ nm, $b=(3.6\pm 0.3)$ nm, and $\alpha=(86\pm 5)^\circ$. A closer inspection reveals additional small bright spots in every second diagonal in between the HBC cores. These spots are attributed to acceptor molecules **3**, since they are only observed if the acceptor is present. As in the case of pure HBC, not all molecules in the second layer can occupy crystallographically equivalent positions due to an interlayer symmetry mismatch.

Figure 6(b) displays the current-voltage characteristics of the HBC cores in the second layer in this architecture. In contrast to the case of pure HBC all HBC molecules appear

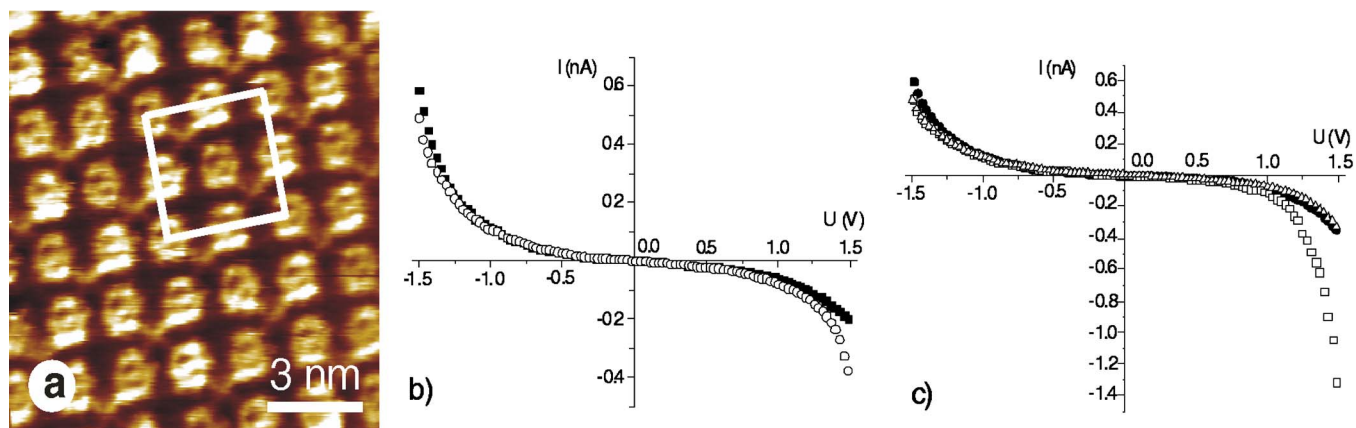


FIG. 6. (Color online) (a) An STM current image of the second layer obtained from an equimolar mixture of **2** and **3** ($U_s=-1.2$ V and $I_t=100$ pA). (b) I-Vs recorded at aromatic cores of **2** (open symbols, average over 39 single curves) in this arrangement compared to the model **1** (solid symbols), (c) as well as I-Vs recorded at the diagonal sites in the oblique arrangement occupied by acceptor molecules (open squares, 32 single curves), empty diagonal sites (open triangles, 46 single curves) compared to I-Vs through alkyl chains of an alkylated HBC (solid symbols).

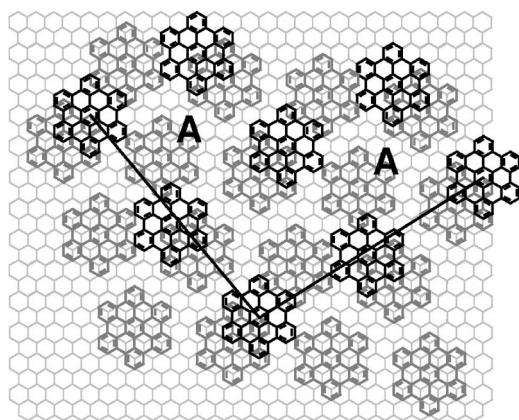


FIG. 7. The packing model for the double layer architecture obtained from equimolar mixtures of **2** and **3**. The first and second layer are depicted in gray and black, respectively. The unit cell, taking into account inequivalent positions with respect to the first layer, is indicated. The positions that are likely, to be occupied by the acceptor are indicated with A.

now to be electronically equivalent within the experimental error. A slightly increased tunneling probability at positive sample bias is observed in comparison to the model **1**. Considering the discussion of the pure HBC case this points towards a lateral offset of the disks in the second layer with respect to the first which is in between the two extremes suggested for the architecture obtained from neat **2**. One also expects a coupling of the HBCs in the second layer to two disks in the first layer with the overlap to the second of two underlying disks being smaller than in the case of the neat HBCs. Figure 6(c) displays the I-Vs obtained from the diagonal sites in the oblique arrangement. The I-Vs at the non-occupied diagonal sites are indistinguishable from the ones obtained previously from the alkyl chains of an alkylated HBC,³⁰ which regions of layers of the model **1**, which suggests that the underlying HBCs are not centered at the intersections of the diagonals of the oblique arrangement. The STS curves measured at the sites occupied by CDI molecules exhibit the typical asymmetry expected for an electron acceptor²⁹ with larger tunneling probability at positive sample bias. However, it should be kept in mind that here the acceptor is embedded in a three-dimensional architecture.

The hexagonally close-packed ground layer of HBC can be modeled as in the case of a neat HBC **2**. The current-voltage characteristics of HBC cores in the architectures obtained from the mixed solutions exhibit a slightly larger tunneling probability at positive sample bias compared to the model **1**. This increase is in between the two extremes observed for neat HBC. Since in that case the increasing tunneling probability was attributed to a coupling to two disks in the first layer due to a larger lateral offset, we now suggest an intermediate offset still with a coupling to two disks. Indeed, it is possible to arrange the HBCs in the second layer such that all have a lateral offset of 0.51 nm with respect to

the HBC on which they stack and a small overlap with its neighbor (Fig. 7). The unit cell in this model with parameters of 3.7 nm, 3.8 nm, and 88° reproduces the experimental values within the experimental error.

As expected, the HBCs do not occupy equivalent positions on the lattice of the first layer, but the electronic coupling is very similar for all of them and obviously not distinguishable within the accuracy of our experiment. The model also explains the adsorption of the electron acceptor in every second diagonal only, apparently the intersection points of the diagonals are not equivalent since the possible couplings to the underlying HBCs are different. Therefore, it is suggested that the molecules of **3** only adsorb at the sites with optimized coupling to the first layer.

A further possible explanation to be considered for the increase in the tunneling probability through the HBC in the second layer is the formation of charge-transfer complexes between the HBCs in the first layer and the electron acceptors. However, the resulting interface dipole pointing towards the substrate would lead to a decrease in tunneling probability.¹⁸ Therefore this explanation is excluded.

IV. CONCLUSIONS

Scanning tunneling microscopy and spectroscopy studies of hexa-*peri*-hexabenzocoronenes (HBCs) in double layers revealed a strong dependence of their electronic properties on the immediate molecular environment. In particular, current-voltage characteristics through HBCs in the second layer differed significantly for the different positions of these molecules with respect to the first layer. Packing models with atomic scale precision (better than 0.1 nm), based upon STM and STS data, indicate that larger lateral offsets between disks in the two layers, corresponding also to coupling between three rather than two disks, result in a relative increase of tunneling probability at positive sample bias. This behavior is attributed to the dependence of HOMO- and LUMO-splitting on the lateral offset in stacked conjugated molecules, as calculated recently. In particular, the increase of tunneling probability is suggested to be caused by the resonant contributions of the LUMO due to a narrowing of the HOMO-LUMO gap upon larger HOMO and LUMO splittings when disks in the second layer couple to two instead of only one disk in the first layer. The results provide strong experimental support to the theoretical predictions that the control over the stacking in short nanographene columns can be used to control their electron transport properties between appropriate contacts.

ACKNOWLEDGMENTS

This work has been supported by the European Union through MAC-MES (Project No. GRD2-2000-30242) and the German Research Foundation (DFG) through Sfb 658 "Elementarprozesse in molekularen Schaltern an Oberflächen."

*Corresponding author: Electronic address: rabe@physik.huberlin.de

- ¹A. Aviram and M. A. Ratner, *Chem. Phys. Lett.* **29**, 277 (1974).
- ²C. Joachim, J. K. Gimzewski, and A. Aviram, *Nature (London)* **408**, 541 (2000).
- ³R. L. Carroll and C. B. Gorman, *Angew. Chem., Int. Ed.* **41**, 4378 (2002).
- ⁴A. Nitzan and M. A. Ratner, *Science* **300**, 1384 (2003).
- ⁵A. Stabel, P. Herwig, K. Müllen, and J. P. Rabe, *Angew. Chem., Int. Ed.* **34**, 1609 (1995).
- ⁶R. M. Metzger, B. Chen, U. Höpfner, M. V. Lakshmikantham, D. Vuillaume, T. Kawai, X. Wu, H. Tachibana, T. V. Hughes, H. Sakurai, J. W. Baldwin, C. Hosch, M. P. Cava, L. Brehmer, and G. J. Ashwell, *J. Am. Chem. Soc.* **119**, 10455 (1997).
- ⁷C. Joachim and J. K. Gimzewski, *Chem. Phys. Lett.* **265**, 353 (1997).
- ⁸P. Samorì, *J. Mater. Chem.* **14**, 1353 (2004).
- ⁹S. De Feyter and F. C. De Schryver, *J. Phys. Chem. B* **109**, 4290 (2005).
- ¹⁰T. W. Kelley, E. L. Granstrom, and C. D. Frisbie, *Adv. Mater.* **11**, 261 (1999).
- ¹¹M. A. Reed, C. Zhou, C. J. Muller, T. P. Burgin, and J. M. Tour, *Science* **278**, 292 (1997).
- ¹²C. Kergueris, J. P. Bourgoin, S. Palacin, D. Esteve, C. Urbina, M. Magoga, and C. Joachim, *Phys. Rev. B* **59**, 12505 (1999).
- ¹³C. Zhou, M. R. Desphande, M. A. Reed, L. Jones, and J. M. Tour, *Appl. Phys. Lett.* **71**, 611 (1997).
- ¹⁴S. Tans, A. R. M. Verschueren, and C. Dekker, *Nature (London)* **393**, 49 (1998).
- ¹⁵J. A. Misewich, R. Martel, Ph. Avouris, J. C. Tsang, S. Heinze, and J. Tersoff, *Science* **300**, 783 (2003).
- ¹⁶H. Park, J. Park, A. K. L. Lim, E. H. Anderson, A. P. Alivisatos, and P. L. McEuen, *Nature (London)* **407**, 57 (2000).
- ¹⁷W. Liang, M. P. Shores, M. Bockrath, J. R. Long, and H. Park, *Nature (London)* **417**, 725 (2002).
- ¹⁸F. Jäckel, M. D. Watson, K. Müllen, and J. P. Rabe, *Phys. Rev. Lett.* **92**, 188303 (2004).
- ¹⁹R. Friedlein, X. Crispin, C. D. Simpson, D. M. Watson, F. Jäckel, W. Osikowicz, S. Marciniak, M. P. de Jong, P. Samorì, S. K. M. Jönsson, M. Fahlman, K. Müllen, J. P. Rabe, and W. R. Salaneck, *Phys. Rev. B* **68**, 195414 (2003).
- ²⁰D. S. Seferos, S. A. Trammell, G. C. Bazan, and J. G. Kushmerick, *Proc. Natl. Acad. Sci. U.S.A.* **102**, 8821 (2005).
- ²¹H. Uji-i, S. Nishio, and H. Fukumura, *Chem. Phys. Lett.* **408**, 112 (2005).
- ²²A. Gesquière, S. De Feyter, F. C. De Schryver, F. Schoonbeek, J. Van Esch, R. M. Kellog, and B. L. Feringa, *Nano Lett.* **1**, 201 (2001).
- ²³A. van de Craats, J. M. Warman, A. Fechtenkötter, J. D. Brand, M. A. Harbison, and K. Müllen, *Adv. Mater.* **11**, 1469 (1999).
- ²⁴M. D. Watson, F. Jäckel, N. Severin, J. P. Rabe, and K. Müllen, *J. Am. Chem. Soc.* **126**, 1402 (2004).
- ²⁵C. D. Simpson, J. Wu, M. D. Watson, and K. Müllen, *J. Mater. Chem.* **14**, 494 (2004).
- ²⁶U. Rohr, P. Schlichting, A. Böhm, M. Gross, K. Meerholz, C. Bräuchle, and K. Müllen, *Angew. Chem., Int. Ed.* **37**, 1434 (1998).
- ²⁷P. Samorì, N. Severin, C. D. Simpson, K. Müllen, and J. P. Rabe, *J. Am. Chem. Soc.* **124**, 9454 (2002).
- ²⁸J. P. Rabe and S. Buchholz, *Science* **253**, 424 (1991).
- ²⁹R. Lazzaroni, A. Calderone, J. L. Brédas, and J. P. Rabe, *J. Chem. Phys.* **107**, 99 (1997).
- ³⁰F. Jäckel, Z. Wang, M. D. Watson, K. Müllen, and J. P. Rabe, *Chem. Phys. Lett.* **387**, 372 (2004).
- ³¹R. Goddard, M. W. Haenel, W. C. Herndon, C. Krüger, and M. Zander, *J. Am. Chem. Soc.* **117**, 30 (1995).
- ³²T. Schmitz-Hübsch, F. Sellam, R. Staub, M. Törker, T. Fritz, C. Kübel, K. Müllen, and K. Leo, *Surf. Sci.* **445**, 358 (2000).
- ³³J. L. Brédas, J. P. Calbert, D. A. da Silva Filho, and J. Cornil, *Proc. Natl. Acad. Sci. U.S.A.* **99**, 5804 (2002).
- ³⁴C. A. Hunter, K. R. Lawson, J. Perkins, and C. J. Urch, *J. Chem. Soc., Perkin Trans. 1* **1**, 651 (2001).